JCE

Journal of Civil Engineering
ISSN 2086 - 1206 E-ISSN 2579 - 9029

Application of Non-Linear Fiber Section Model on Spun Piles With and Without Concrete Infill Subjected to Cyclic Loading

Estu E. Apriliana[a], Candra Irawan[a*], Priyo Suprobo[a]

Correspondence

[a]Department of Civil Engineering, Sepuluh Nopember Institute of Technology (ITS), Surabaya 60111, Indonesia.

Corresponding author email adress: chandra@ce.its.ac.id

Submitted : 17 May 2024
Revised : 13 June 2024
Accepted : 14 June 2024

Abstract

This numerical analysis study predicts the behavior of spun piles with and without concrete infill under cyclic flexural loading and constant axial load. A fiber section using STKO pre- and post-processor for the OpenSEES program was employed. Spun piles were modeled using displacement-based beam-column elements with distributed plasticity and cyclic loading procedures with displacement control. The numerical method proposed for this research was verified by comparing it to reliable experimental results.

Keywords
Spun pile, fiber section, distributed plasticity, cyclic loading

INTRODUCTION

The spun pile is a hollow prestressed concrete pile widely used as foundations or columns in buildings, bridges, and wharves to obtain a more economical design alternative and provide high effectiveness of section properties. However, spun piles have some disadvantages, such as low energy dissipation, low ductility, and sudden or brittle collapse behavior[1], [2], [3]. Figure 1 shows the difference in the stress–strain relationship between confined and unconfined concrete, where confined concrete exhibits larger strength and ductility than unconfined concrete. This enhanced strength and ductility of confined concrete depends on the confining pressure. The confining pressure can be controlled using outer transverse reinforcements in a general RC column. In a spun pile, however, the confining pressure may not be controlled by only the outer
transverse reinforcements because there is no confining pressure at the inner face of the column, which causes low ductility and low energy dissipation [4]. To address this weakness, Irawan 2019 [5] added concrete infill to the spun pile to create radial restraint on the inner concrete wall to increase the ductility value.

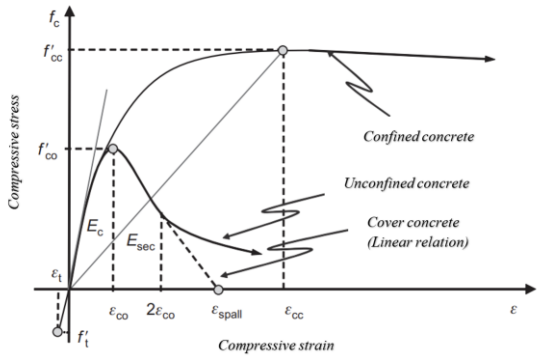

Figure 1 Stress-strain relationship of restrained and unrestrained concrete [6]

RESEARCH SIGNIFICANCE

The objective of this study is to create a numerical model to predict the behavior of spun pile with and without concrete infill due to cyclic bending loads and constant axial loads. Fiber section model using STKO pre- and post-processor for OpenSEES were performed. The numerical analysis results were verified in the experiment carried out by Irawan 2019 [5].

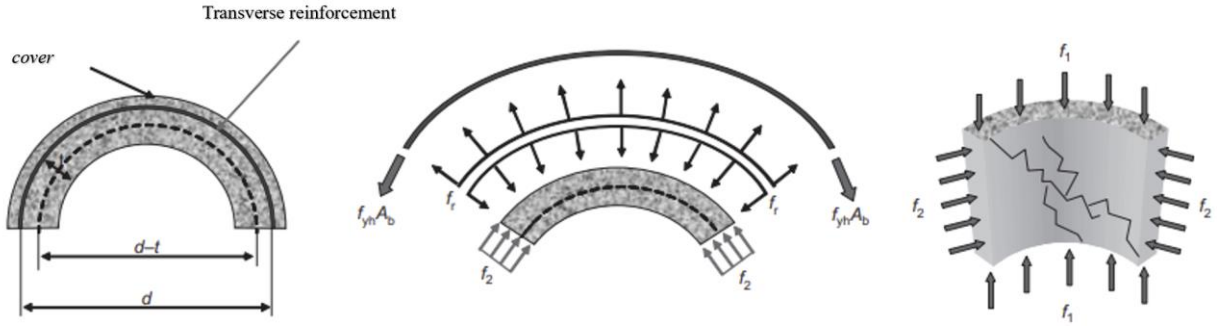

Figure 2 Illustration of biaxial restraint in spun pile concrete [4]

METHODOLOGY

The research methodology in this paper is divided into four stages: 1) Collecting specimen data from previous research [5]. 2) Determination of input parameters for unconfined concrete, confined concrete, and steel materials. 3) Implement a modeling strategy for spun pile with and without concrete infill. 4) Evaluating the behavior of each specimen.

A. STRESS-STRAIN RELATIONSHIP OF CONFINED CONCRETE IN SPUN PILE

The concrete wall element in Figure 2 is biaxially confined by axial stress (*f1*) and circumferential stress (*f2*). In this case, the brittle failure originates from the inner surface of the column. The constitutive model of confined concrete for spun pile follows the study conducted by [4] which explains that the transverse reinforcement in Figure 2 does not provide lateral pressure on the core concrete in the radial direction, there is only circumferential stress which acts curved on the concrete.

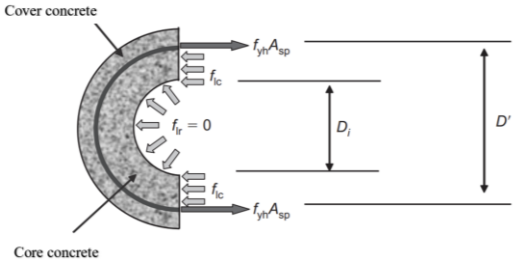

Figure 3 *Confining stress* in *spun pile* concrete [4]

The circumferential confining pressure (*flc*) can be calculated using the same method as generally applied to solid reinforced concrete. The confining stress in the radial direction (*flr*) is assumed to be 0 (f_{lr} = 0). From the assumption of f_{lr} =*0* and $f_{lc} \neq 0$, the concrete in a hollow spun pile member can be considered to be in the state of biaxial confinement, and the effective lateral pressure (f_1') at the yield can be defined as the average of radial and circumferential confining stress components (f_{lr}) and (f_{lc}) as specified by equation 2.

$$2f_{lc}(D' - D_i)s = 2f_{yh}.A_{sp} \rightarrow f_{lc} = \frac{2f_{yh}.A_{sp}}{(D'-D_i)s} \quad (1)$$

$$f_1' = 0.5(f'_{lr} + f'_{lc}) \quad (2)$$

Where $f'_{lc} = 0.95f_{lc}$[8]. D' is the diameter of the confined concrete core, *Di* is the inner diameter of the spun pile, f_{yh} is the yield stress of transverse reinforcement, and A_{sp} is the cross-sectional area of the transverse reinforcement.

The confined concrete compressive strength for columns with hollow sections developed by [4] based on the one proposed by [8] are as follows:

$$f'_{cc} = -2.75\frac{f_1'^2}{f_c'} + 1.835\, f_1' + f_c' \quad (3)$$

The strain at the point of maximum stress was determined using the following equation.

$$\varepsilon_{cc} = \varepsilon_{c0}\left[1 + 5\left(\frac{f'_{cc}}{f'_{c0}} - 1\right)\right] \quad (4)$$

B. STRESS-STRAIN RELATIONSHIP OF CONFINED CONCRETE IN SPUN PILE WITH CONCRETE INFILL

The concrete wall element of the filled spun pile in Fig. 4 is triaxially confined by axial stress (*f1*), circumferential stress (*f2*) and radial stress (*f3*). The infill concrete offers confining stress in the radial direction. The spun pile with infill concrete produces more strength and ductility than the spun pile without infill concrete.

Confining pressure in the circumferential and radial directions are considered equal (*flc* = *flr*). Based on the analysis conducted by [9] regarding the behavior of the interface between the spun pile element and the concrete infill and from [5] in calculating the shrinkage of infill concrete, the infill concrete used in the experiment exhibits shrinkage strain that does not significantly affect the stress-strain characteristics of concrete. Additionally, the interface element shows frictional stress despite the time difference in casting time between the spun pile and the infill concrete, Hence, the spun pile and infill concrete components are considered as a single cross-sectional unit. The peak concrete strength for confined concrete (f'_{cc}) in spun pile cores was conducted using the equation proposed by [8] as follows:

$$f'_{cc} = f'_{co}\left(-1.254 + 2.254\sqrt{1 + \frac{7.94f_1'}{f'_{co}}} - 2\frac{f_1'}{f'_{co}}\right) \quad (5)$$

Where *fl'* is the effective lateral pressure obtained from [8], and *f'co* is the unconfined concrete compressive strength. The strain at the point of maximum stress is calculated using Equation 4.

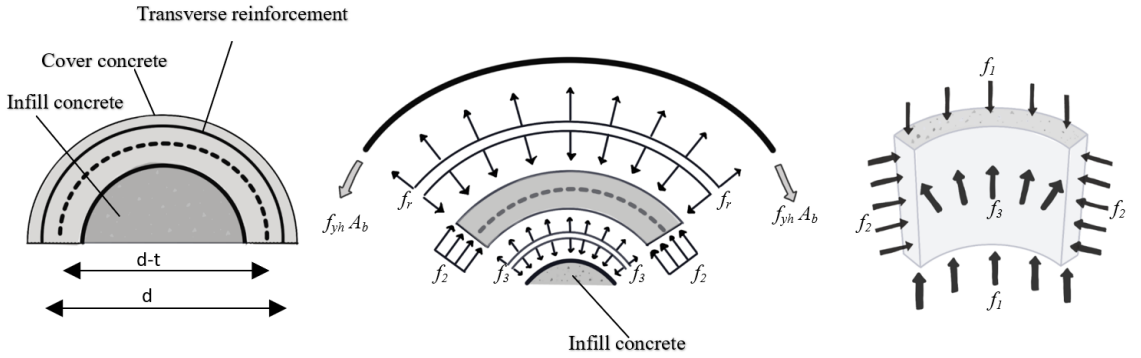

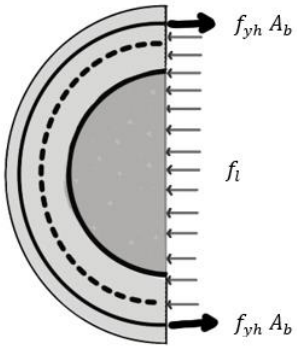

Figure 5 *Confining stress* in spun pile concrete with concrete infill

C. OPENSEES COMPUTATIONAL PLATFORM

Open System for Earthquake Engineering Simulation (OpenSees) [10] is an open-source computational platform for conducting structural and geotechnical simulations using finite element methods. The main advantage of this software is the flexibility in modelling structural or geotechnical components at different stages i.e., by using a force-deformation behavior at the element level, using a moment-curvature behavior at the section level, and using material stress-strain behavior at the fiber level, [11].

OpenSees commonly utilizes various uniaxial materials for structural simulations, including elastic materials, elastic-perfect plastic materials, and more. The widely used uniaxial concrete material models are concrete01, concrete02, concrete04, and concrete07. Similarly, steel materials are represented by models such as steel01, steel02, Reinforcing Steel, and many others [10].

The section level is employed to characterize the force magnitude that causes deformation in a beam-column section; for example, the moment-curvature relationship can be defined at a cross-section of a beam-column using a *section* command. Elastic, Fiber, and Uniaxial section definitions are among the various types available. The Fibre model allows biaxial bending interaction with an axial force acting simultaneously. The Fiber section command is especially noteworthy as it discretizes the cross-section into a collection of fibers, each representing a uniaxial stress-strain material response. When applied to reinforced concrete (RC), basic quadrilateral shapes can be established using the patch command for the concrete portion and the layer command for reinforcement bars. The accuracy of the response and the computational cost depends upon the optimal number of fibers used for discretization [11].

At *Element models,* several options are available for the element-level formulation for force deformation. Typical elements used for numerical analysis include *truss*, *elastic Beam Column*, *nonlinear Beam Column*, *zero Length*, *quad*, *shell*, *brick*, and *link* elements among several others. For the application to reinforced concrete, the elements of interest are *elastic Beam Column* and *nonlinear Beam Column* elements for simulating the beam and column component response. There are primarily two types of nonlinear beam-column element models, force based element (FBE) and displacement-based element (DBE). An FBE (*force Beam Column*) formulation satisfies the equilibrium between element and section forces in the strong form for the range of constitutive nonlinearity. It adopts the principle of virtual forces for formulating compatibility between section and element deformations [11]. On the other hand, DBE (*disp Beam Column*) uses standard finite element procedures to interpolate section deformations from approximate displacement field and then adopts principle of virtual deformations to form an element equilibrium relationship. Detailed theoretical aspects of these elements are discussed in [12].

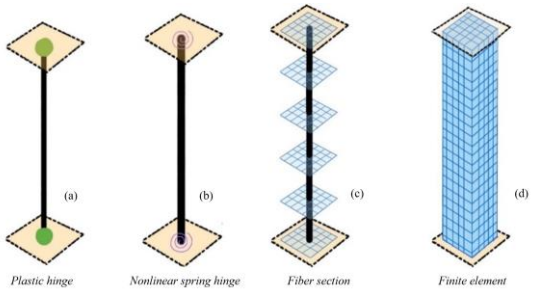

Figure 6 Idealization type of plasticity modeling

Figure 6 illustrates various modeling approaches to simulate the nonlinear response mechanism of a structural element. As seen in Figure 6 (a) and (b), which is a Concentrated Plasticity (CP) model having linear elastic interior portions combined with one rotational spring at each end, plastic deformation occurs in plastic hinges, while other parts of the element remain elastic. Figure 6 (c) is a Distributed Plasticity (DP) model showing the plasticity zone spread along the length of the element. The force-displacement response to an element is obtained from numerical integration at discrete points called integration points along the element. In the *OpenSees* program, several integration schemes are available, such as Gauss-Lobatto, Gauss-Legendre, and Gauss-Radau. The Distributed Plasticity approach is effective for stable numerical analysis because it integrates the cross-sectional response (section) and the fiber section command, allowing for rational interaction between axial and bending behavior along the element. Figure 6 (d) presents a simulation approach with a continuum model as the most reliable model for seismic behavior demand, however, typically complex and leads to extensive computational cost. [11].

D. DESCRIPTION OF TEST SPECIMENS

This study used the data for spun pile with and without infill concrete under constant axial and cyclic load as proposed by [5] to verify the applicability of the proposed method. All specimens had the exact section dimensions of 400 mm diameter with 100 mm thick walls (Fig.5). four specimens of the spun pile were constructed and tested under axial compression and cyclic flexure. The material properties of the specimens are listed in Table 1, and specimen names in the tables are those used by [5].

Table 1 List of specimens

Test Specimens	*fc'* (MPa)		*fy* (MPa)		*Axial Load*
	Pre-cast concrete	Concrete infill	PC bar	*Spiral wire*	
S-TB-1	54.4	-	1387	681	0.08 *fc' Ag*
S-TB-3	54.4	-	1387	681	0.16 *fc' Ag*
S-DB-1	54.4	33	1387	681	0.08 *fc' Ag*
S-DB-3	54.4	33	1387	681	0.16 *fc' Ag*

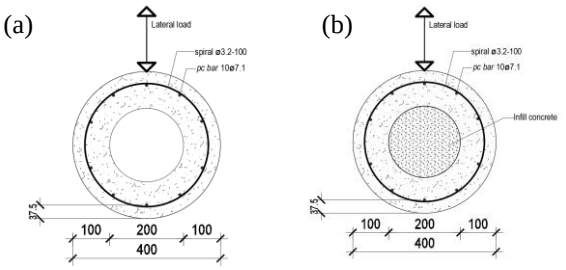

Figure 7 Test specimens of spun piles; (a) spun piles without concrete infill (S-TB-1 and S-TB-3); (b) spun piles with concrete infill (S-DB-1 and S-DB-3) [5]

E. DESCRIPTION OF ANALYTICAL MODEL

The fiber section model for the spun pile was proposed based on the OpenSees platform, as shown in Fig. 8(a). The height of the specimen was 3500 mm, divided into four elements. To illustrate how the material nonlinearity is distributed along the height, fiber sections and nonlinear displacement-based beam-column elements with three integration points have been applied in the models. The fiber section was defined separately into cover concrete, core concrete, and PC bar with proper uniaxial stress-strain models. The cover and core concrete were modeled based on the constitutive model proposed by Yassin [61] (labeled as '*Concrete02*' model in OpenSees). The input parameters of concrete02 were compressive strength (fpc), concrete strain at maximum strength ($\varepsilon psc0$), concrete crushing strength ($fpcu$), concrete strain at crushing strength (εpsU), the ratio between unloading slope at $epsc0$ and initial slope (λ), tensile strength (ft) and tension softening stiffness (Ets) [11]. The concrete compressive strength and corresponding strain values of confined concrete are calculated according to the confined concrete model proposed by Mander et al. [62]. The strain value when the first stirrup fractures is adopted as the ultimate compressive strain of confined concrete (εcu) for the core of spun pile with infill concrete, which is proposed by Priestley et al. [63], as shown in Equation (6), Meanwhile, the ultimate compressive strain (εcu) for spun pile without infill concrete is taken based on Coleman & Spacone [11], as shown in Equation (7).

- *spun pile* with concrete infill

$$\varepsilon_{cu} = 0.004 + 0.14 \cdot \rho_s \cdot \frac{f_{ys}}{f_c'} \qquad [8] \qquad (6)$$

Where ρ_s is the transverse reinforcement ratio, f_{ys} is the yield stress of transverse reinforcement, and f_c' is the maximum unconfined compressive strength of concrete.

- *Spun pile* without concrete infill

$$\varepsilon_{cu} = \frac{G_f^c}{0.6\, f_c'\, L_{IP}} - \frac{0.8\, f_c'}{E_c} + \varepsilon_{co} \qquad [14] \qquad (7)$$

Taking the fracture energy of the concrete (G_f^c)=20 N/mm (based on the recommendation by Jansen and Shah 1997 [15]), Lip denotes the length of the integration point on the element, which can be approximated as the length of the plastic hinge (L_p) [14], As the test specimens in this study were analyzed under significant axial loads, the value of Lip ≈ Lp ≈ 1.0h was chosen, following the formulation [15], where h represents the diameter of the spun pile.

Steel02 material based on the Giuffre-Menegotto-Pinto model was adopted to construct the behavior of the PC bar. The input parameters were yield strength (*fy*), initial elastic tangent (E_0), strain-hardening ratio (b), and the parameters to control the transition from elastic to plastic branches (R0, cR1, cR2). Initial stress material was adopted to develop the PC bar pre-tensioning effect with a magnitude of 1101 MPa. The material modeling and the parameters are shown in Table 2 and Table 3.

1.

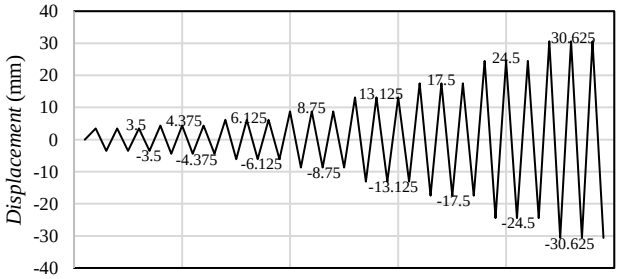

Figure 9 The lateral cyclic loading cycle

RESULTS AND DISCUSSIONS

A. ANALYSIS AT THE ELEMENT LEVEL

Figure 10 shows the hysteresis loops for load versus displacement at the loading point. The analytical results show reasonable agreement with the experimental results. It can be found from the figure that the load–displacement curve is approximately linear before cracking, the displacement develops linearly, and the residual deformation after unloading is very small.

The analysis not only correctly predicted the load and deformation at the peak but also captured the post-peak softening well. The predictions of the failure modes of all specimens also agree with the experimental results.

Table 2 The parameters of concrete

Parameter Concrete02	*Cover*	*Core**	*Core***	*Infill*
$f_{pc}\ (MPa)$	$f_c' = 54.4$	$f_{cc}' = 55.18$ (pers. 3)	$f_{cc}' = 56.36$ (pers. 5)	$f_{cc}' = 34.112$
ε_o	0.0022	$\boldsymbol{\varepsilon_{cc}} = 0.00235$ (pers.4)	$\boldsymbol{\varepsilon_{cc}} = 0.002597$ (pers.4)	$\boldsymbol{\varepsilon_{cc}} = 0.00257$ (pers.4)
$f_{cu}\ (MPa)$	0	$0.2xf_{cc} = 11.034$	$0.2xf_{cc} = 11.27$	$0.2xf_{cc} = 6.62$
ε_{cu}	0.00248 (pers. 7)	0.002604 (pers. 7)	0.00511 (pers. 6)	0.0058 (pers. 6)
λ	0.1	0.1	0.1	0.1
$f_t(MPa)$	$0.04f_c' = 2.176$	$0.04f_{cc}' = 2.207$	$0.04f_{cc}' = 2.254$	$0.04f_{cc}' = 1.364$
$E_{ts}(MPa)$	$f_t/\varepsilon_o = 989.091$	$f_t/\varepsilon_{cc} = 926.060$	$f_t/\varepsilon_{cc} = 968.078$	$f_t/\varepsilon_{cc} = 513.425$

* *spun pile* concrete core without infill

** *spun pile* concrete core with infill

Table 3 The parameters of PC metal bar

Parameter Steel02	$f_y\ (MPa)$	$E_0\ (MPa)$	b	R_0	c_{R1}	c_{R2}	*Initial Stress*	*Max strain*	*Min Strain*
Pc bar	1404	229577	0.018	18.5	0.925	0.15	0.005	0.01252	-0.01252

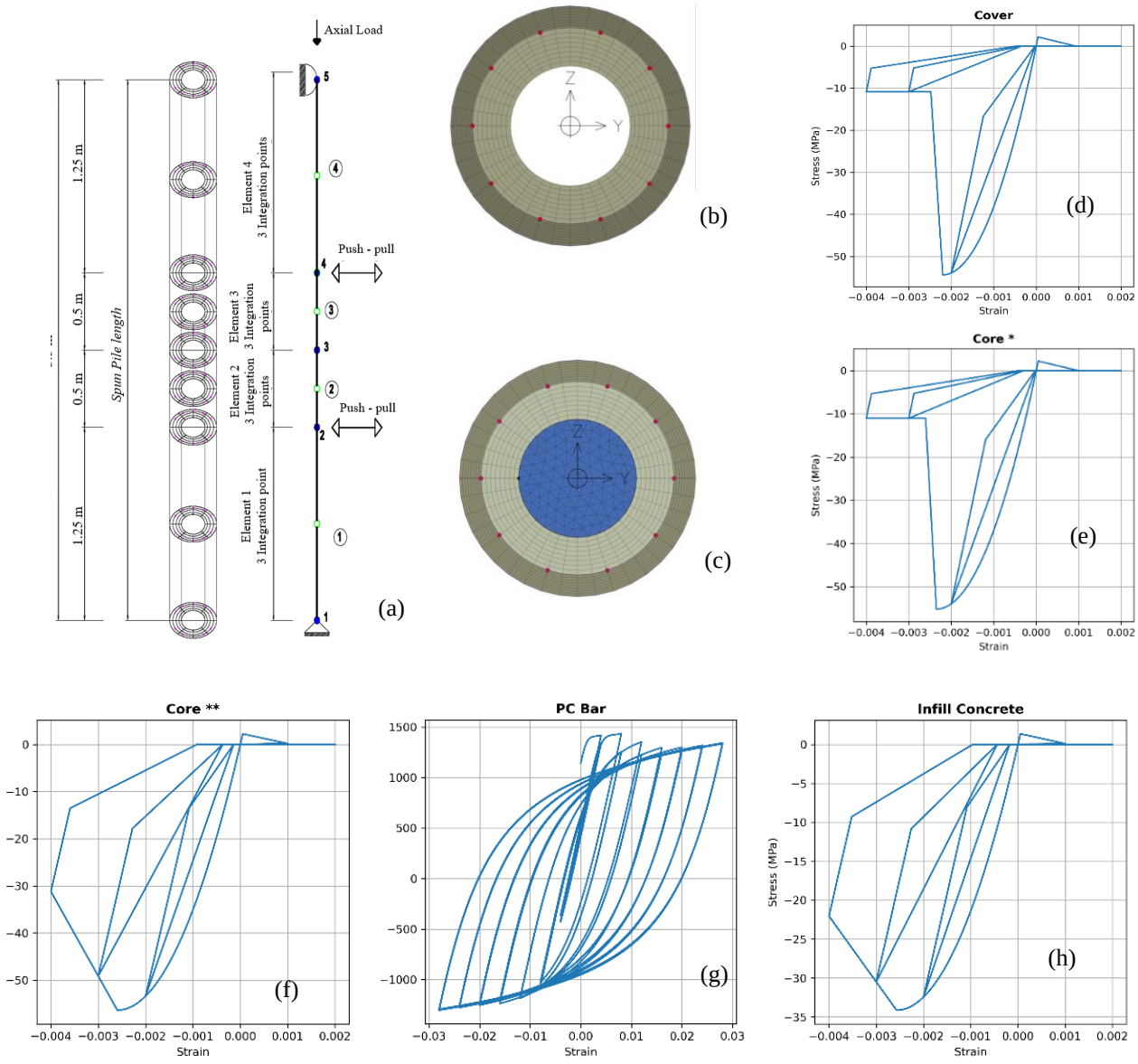

Figure 8 a). Idealization of the spun pile test specimen; b) Fiber section of spun piles S-TB 1 & 3; c) Fiber section of spun piles S-DB 1 & 3; d) Model material for concrete cover; e) Model material for concrete core of S-TB 1 & 3; f) Model material for concrete core of S-DB 1 & 3; g) Model material for PC bar; h) Model material for concrete infill.

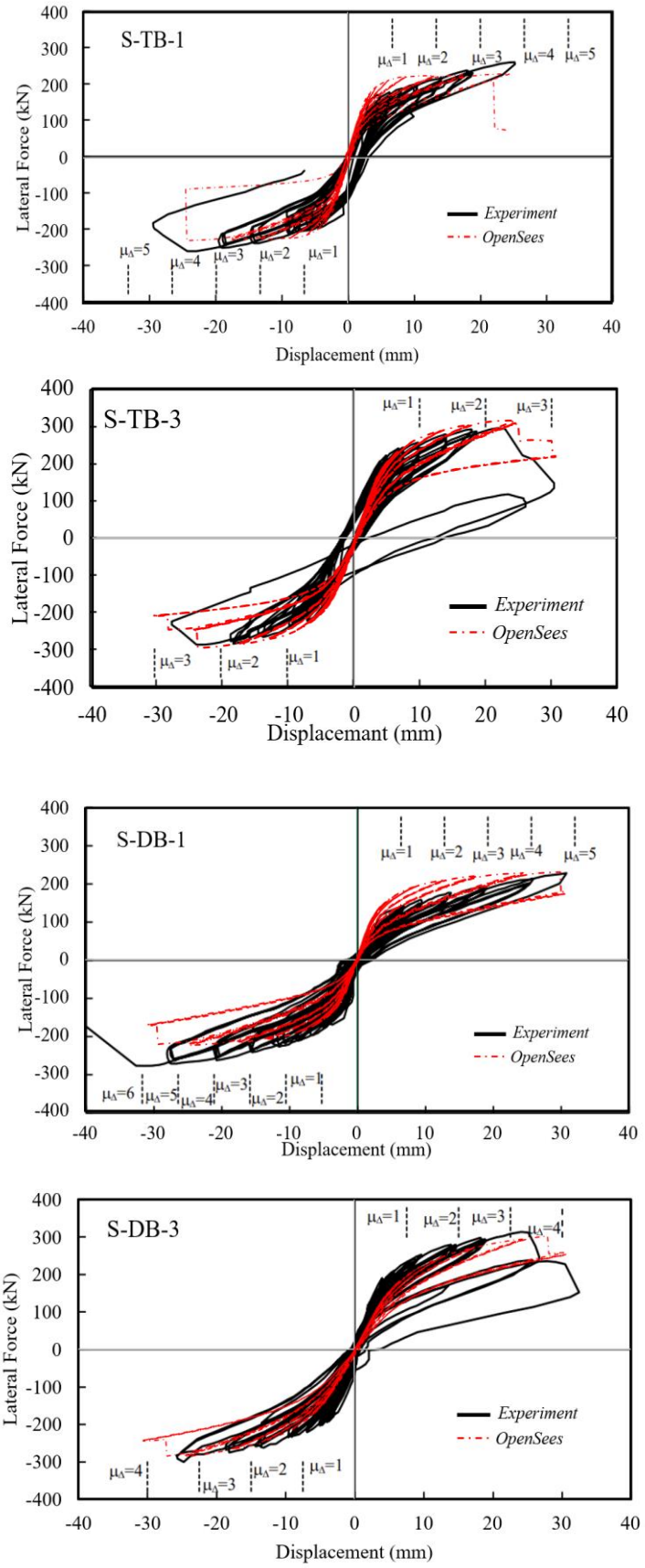

Figure 10 The *displacement -lateral force curve for every spun file specimen*

Table 4 Ultimate lateral load of spun pile from experiments and *OpenSees* model.

Specimen	Lateral Loading (kN)		Exp/Model
	Experiment	Model *OpenSees*	
S-TB-1	261	231	1.13
S-TB-3	296	313	0.95
S-DB-1	277	232	1.19
S-DB-3	314	303	1.04

B. ANALYSIS AT FIBER-LEVEL

Figure 11 depicts the strain-displacement relationship curves for the PC bar on the specimen's front and back sides. Notably, the PC bar exhibits an initial prestressed strain of 0.005. The maximum strain observed in the PC bar reached 0.012 in all test specimens. This indicates that the PC bar experienced tensile failure when the displacement values reached 22mm and 23mm, 26mm and 28mm, 24mm, and 24mm, and 30mm and 30mm on the back and front sides, respectively. These observations are related to the specimens S-TB-1, S-TB3, S-DB-1, and S-DB-3, respectively.

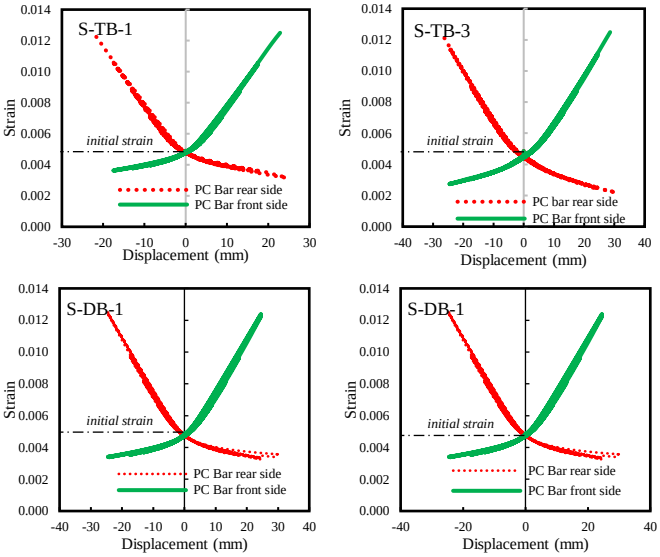

Figure 11 Strain-displacement curve of PC bar from numerical analysis

The numerical analysis verification results of the strain-displacement curve for the PC bar were compared with experimental data as conducted by [5]. In the experiment, a strain gauge was employed to measure strain values. Still, it was installed after subjecting the PC bar to prestressed forces, making it impossible to obtain the initial strain value directly. Therefore, to align the numerical analysis results with the experimental strain-displacement curve, it was necessary to subtract the initial strain value of 0.005. Figure 12 demonstrates that the strain-displacement relationship curve obtained from *OpenSees* closely resembles the curve derived from the experimental results, verifying the accuracy of the numerical analysis.

The strain-displacement relationship is depicted in Figure 14, revealing that during the initial testing phase, the concrete underwent compressive strains due to prestressing and axial loads. Specifically, the specimens S-TB-1, S-TB3, S-DB-1, and S-DB-3 exhibited compressive strains of 0.00019, 0.00042, 0.00017, and 0.00053, respectively.

As the testing progressed, all test specimens reached a critical crushing strain value of -0.00248. This occurred when the specimens experienced displacements of 23mm and 18mm for specimen S-TB-1, 14mm and 14mm for S-TB3, 20mm and 19mm for S-DB-1, as well as 10mm and 12mm for the front and rear sides of S-DB-3, respectively.

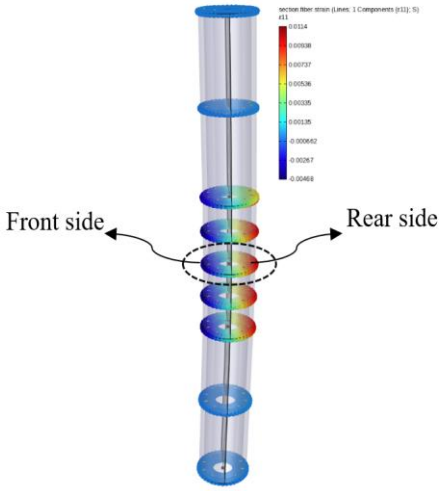

Figure 12 Fiber section analysis of test specimen S-TB-1

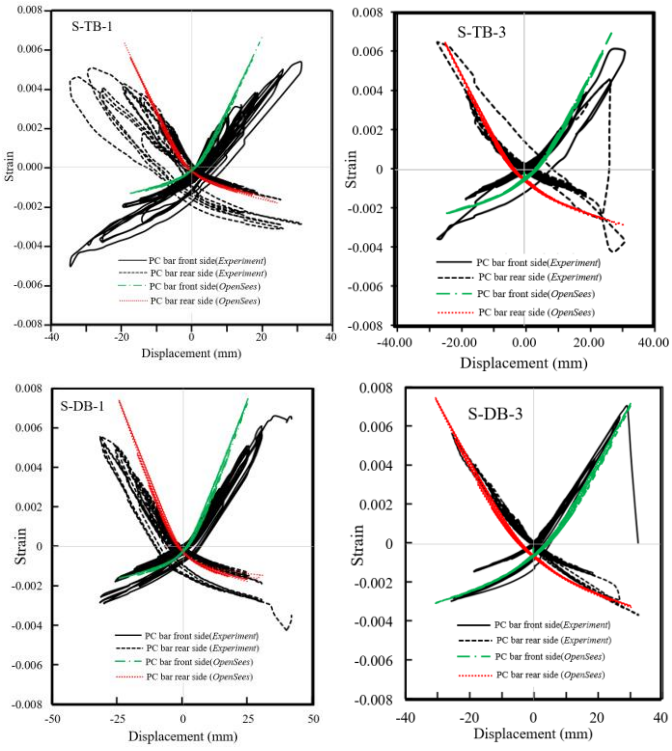

Figure 13 Strain-displacement curve of the PC bar

Table 5 Displacement of the test specimen at failure from the OpenSees analysis

Test specimen	*Displacement when the PC bar ruptures*		*Displacement when the concrete cover is crushed*		Remarks
	Front side	Rear Side	Front side	Rear side	
	mm	mm	mm	mm	
S-TB-1	22	23	23	**18**	Concrete crushed first
S-TB-3	26	28	**14**	**14**	Concrete crushed first
S-DB-1	24	24	20	**19**	Concrete crushed first
S-DB-3	30	30	**10**	**10**	Concrete crushed first

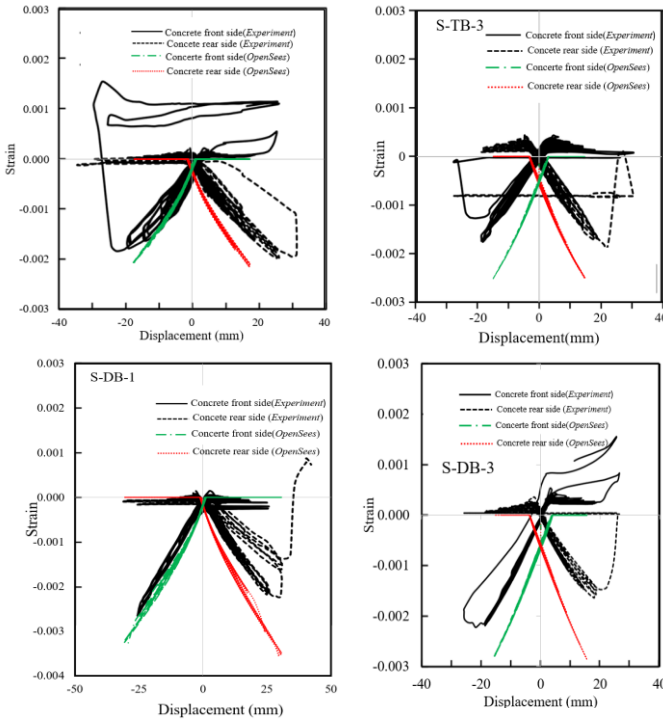

Figure 14 Strain-displacement curve of the concrete cover

Figure 14 presents the strain-displacement relationship, highlighting that the concrete underwent compressive strains during the initial testing phase due to prestressing and axial loads. Specifically, specimens S-TB-1, S-TB3, S-DB-1, and S-DB-3 exhibited compressive strains of 0.00019, 0.00042, 0.00017, and 0.00053, respectively. All test specimens ultimately reached a critical crushing strain value of -0.00248. This critical point was reached when the specimens experienced displacements of 23mm and 18mm for specimen S-TB-1, 14mm and 14mm for S-TB3, 20mm and 19mm for S-DB-1, as well as 10mm and 12mm for the front and rear sides of S-DB-3, respectively.

Table 6 Displacement of the test specimen at failure from the experimental results

Test specimen	*Displacement when the PC bar ruptures*		*Displacement when the concrete cover is crushed*		Remarks
	Front side	Rear Side	Front side	Rear Side	
	mm	mm	mm	mm	
S-TB-1	-	-	24.5	-	Concrete crushed first
S-TB-3	-	-	**30.6**	**24.5**	Concrete crushed first
S-DB-1	-	-	30.6	-	Concrete crushed first
S-DB-3	-	-	**24.5**	-	Concrete crushed first

Conclusions

This paper presents a comprehensive investigation into modeling and cyclic loading analysis of spun pile piles, both with and without concrete infill, to evaluate the capabilities of the OpenSees computational platform. Experimental data from [5] were employed to validate the accuracy of numerical analysis in predicting the load capacity and load-deformation response of spun piles. The primary findings of this study can be summarized as follows:

1. The material models used in modeling restrained and unrestrained concrete and PC bar steel in this research

have proven to yield satisfactory results for investigating the behavior of spun pile columns under cyclic loading.

2. The proposed fiber section's method can provide predictions for maximum load capacity and displacement-strain curves that closely resemble experimental results and the failure patterns in each test specimen.
3. Analysis at the element level using the Displacement Beam-Column Element can reasonably predict the cyclic load-deformation response and the post-peak behavior of spun piles, indicating a sudden collapse shortly after reaching the maximum load.
4. Analysis at the fiber level provides more detailed outputs, allowing stress and strain values to be extracted from each fiber, facilitating an assessment of the behavior of each material within a section

References

[1] A. M. Budek, G. Benzoni, and M. J. N. Priestley, "Experimental Investigation of Ductility of In-Ground Hinges in Solid and Hollow Prestressed Piles," Structural Systems Research, University of California, 1997.

[2] A. Budek and G. Benzoni, "Obtaining ductile performance from precast prestressed concrete piles," PCI Journal, vol. 54, no.3, pp. 64-30, June 2009.

[3] C. Irawan, R. Djamaluddin, I. G. P. Raka, Faimun, P. Suprobo, and Gambiro, "Confinement behavior of spun pile using low amount of spiral reinforcement - An experimental study," International Journal on Advanced Science, Engineering and Information Technology, vol. 8, no. 2, pp. 501–507, 2018, doi: 10.18517/ijaseit.8.2.4343.

[4] T. H. Han, N. H. Lim, S. Y. Han, J. S. Park, and Y. J. Kang, "Nonlinear concrete model for an internally confined hollow reinforced concrete column," Magazine of Concrete Research, vol. 60, no. 6, pp. 429–440, Aug. 2008.

[5] C. Irawan, P. Suprobo, I. G. P. Raka, and R. Djamaluddin, "Kontribusi Beton Pengisi Terhadap Peningkatan Kinerja Tiang Pancang Spun Pile Akibat Beban Lateral Siklik dan Aksial Tekan," Doctoral thesis, Institut Teknologi Sepuluh November, Surabaya, 2019.

[6] S. Popovics, "A numerical approach to the complete stress-strain curve of concrete," Cement and Concrete Research, vol. 3, no. 5, pp. 583–599, Sep. 1973.

[7] M. Petracca, F. Candeloro, and G. Camata, "STKO user manual." ASDEA Software Technology, Pescara, Italy, 2017.

[8] J. B. Mander, M. J. N. Priestley, and R. Park, "Theoretical Stress-Strain Model For Confined Concrete," Journal of Structural Engineering, vol. 114, no. 8, Aug. 1988.

[9] C. Irawan, P. Suprobo, Faimun et. al, "Studi Geser Friksi Sambungan Tiang Pancang Spun Pile dengan Pile Cap," Institut Teknologi Sepuluh November, Surabaya, June 2013.

[10] S. Mazzoni, F. McKenna, M. H. Scott, and G. L. Fenves, "OpenSees Command Language Manual." Open System for Earthquake Engineering Simulation (OpenSees), July 2006.

[11] J. C. Sunil and P. Kamatchi, "Nonlinear modelling strategies for seismic performance evaluation of reinforced concrete structures," in Materials Today Proceedings, vol. 65, no.3, Mar. 2022.

[12] S. Li, C.-H. Zhai, and L.-L. Xie, "Evaluation of Displacement-Based, Force-Based and Plastic Hinge Elements for Structural Non-Linear Static Analysis," Advances in Structural Engineering, vol. 15, no. 3, pp. 477-488, Mar. 2012.

[13] D. C. Kent and R. Park, "Flexural members with confined concrete," Structural Division, pp. 1964–1990, 1971.

[14] J. Coleman and E. Spacone, "Localization Issues in Force-Based Frame Elements," Journal Of Structural Engineering, vol. 127, no. 11, Nov. 2001.

[15] Shamim. A. Sheikh and Shafik. S. Khoury, "Confined Concrete Columns with Stubs," ACI Structural Journal, vol. 90, no. 4, pp. 414–430, 1993.